

Low-Luminosity Active Galactic Nuclei: Are They UV-Faint and Radio Loud?

Dan Maoz^{1*}

¹*School of Physics and Astronomy, Tel-Aviv University, Tel-Aviv 69978, Israel*

26 May 2019

ABSTRACT

Low-luminosity active galactic nuclei (AGNs) are perceived to be radio loud and devoid of a “big blue bump”, indicating a transition from a radiatively efficient, geometrically thin, accretion disc in high-luminosity AGNs, to a geometrically thick, radiatively inefficient accretion flow at low luminosities and accretion rates. I revisit the issue of the spectral energy distributions (SEDs) of low-luminosity AGNs using recently published, high-angular-resolution data at radio, ultraviolet (UV), and X-ray wavelengths, for a sample of 13 nearby galaxies with low-ionization nuclear emission-line region (LINER) nuclei. I show that, contrary to common wisdom, low-luminosity AGNs have significant nonstellar UV flux, and UV/X-ray luminosity ratios similar, on average, to those of Seyfert 1 nuclei $\sim 10^4$ times more luminous. The α_{ox} index that quantifies this ratio is in the range between -0.8 to -1.4, and is below the extrapolation to low luminosities of the relation between α_{ox} and UV luminosity observed at higher luminosities. In terms of radio loudness, most of the LINERs are indeed radio loud (or sometimes even “super radio loud”) based on their radio/UV luminosity ratios, when compared to the most luminous quasars. However, the entire distribution of radio loudness has been shown to shift to higher radio/UV ratios at low AGN luminosities. In the context of this global shift, some LINERs (the majority) can be considered radio quiet, and some (from among those with black hole masses $\gtrsim 10^{8.5} M_{\odot}$) are radio loud. The SEDs of low-luminosity ($\sim 10^{40} \text{ ergs s}^{-1}$) AGNs are thus quite similar to those of Seyferts up to luminosities of $\sim 10^{44} \text{ ergs s}^{-1}$, and there is no evidence for a sharp change in the SED of AGNs at the lowest luminosities. Thin AGN accretion discs may therefore persist at low accretion rates, in analogy to some recent findings for Galactic stellar-mass accreting black holes.

Key words: galaxies: active — galaxies: nuclei — galaxies: Seyfert – quasars: general – Ultraviolet: galaxies –

1 INTRODUCTION

Supermassive black holes (BHs), whose existence has been postulated since the discovery of quasars, are now believed to reside in the nuclei of all massive galaxies, with a correlation between the masses of the BHs and the masses of their host bulges (as evidenced by the stellar luminosities or the velocity dispersions of the bulges; e.g., Häring & Rix 2004; Tremaine et al. 2002). Following an argument by Soltan (1982), the active galactic nucleus (AGN) luminosity density from recent X-ray and optical surveys, integrated over cosmic time, when compared to the present-day space density of nuclear BHs, provides strong evidence that the BHs have grown primarily during relatively brief ($\sim 10^8 \text{ yr}$) active periods when they accreted in a radiatively efficient

mode as Seyfert nuclei and quasars (Marconi et al. 2004; Shankar et al. 2004). The favored mechanism for achieving the required high rest-mass-to-energy conversion efficiencies ($\epsilon \approx 0.1$) is a geometrically thin, optically thick, accretion disc (Shakura & Sunyaev 1973). A less efficient accretion mode during the Seyfert/quasar phase would overpredict the currently observed BH space density. Semi-direct evidence for the existence of such discs in AGNs has come from the presence of an optical to ultraviolet (UV) “big blue blump” in the spectral energy distributions (SEDs) of luminous AGNs (e.g., Shang et al. 2005; Kishimoto et al. 2005) – presumably the thermal radiation from the disc (Shields 1978; Malkan 1983), as well as from the profiles of iron X-ray emission lines, interpreted as gravitationally redshifted and relativistically Doppler-broadened and -boosted emission from the inner regions of the disc (see Nandra et al. 2006, for a recent review). Estimates of the BH masses in

* E-mail: maoz@wise.tau.ac.il

Seyferts and quasars indicate, furthermore, that the thin discs are often radiating at luminosities near the Eddington limit, L_E , corresponding to the BH mass (Kaspi et al. 2000; Kollmeier et al. 2006; Netzer & Trakhtenbrot 2007).

Compared to the radiatively efficient, high-rate, accretion mode of BHs in their short-lived, high-luminosity, phases, much less is known about BH behavior during their long, quiescent, stages. In the presence of a central BH, and given the ubiquity of gas from the mass loss accompanying normal stellar evolution of the bulge population, it appears unavoidable that accretion on to the BH at some finite rate still takes place (e.g., Soria et al. 2006a,b). However, it has been a challenge to explain how this accretion can be accompanied by only the feeble radiative signatures that are observed in non-active galaxies. During their quiescent stage, BHs may switch to a different accretion mode, characterized by a low accretion rate and low-radiative efficiency. In most models of such radiatively inefficient accretion flows (RIAFs; see, e.g., Yuan 2007, and references therein), the kinetic energy associated with the gas is either advected with the matter into the BH, or redirected into an outflow. The funnels in the geometrically thick structures, such as tori, invoked by such models, also provide a plausible mechanism for collimating axial outflows and jets. Observationally, AGNs show some evidence for a transition from a low-accretion-rate state, with an associated low luminosity and a hard X-ray spectrum, to a high-accretion-rate, high luminosity, soft-X-ray state, analogous to behavior observed in Galactic stellar-mass accreting BHs (e.g., Done & Gierliński 2005). However, direct observational evidence for the existence of RIAFs has been sparse, and some authors have argued against such structures based on the observed spectral slopes in specific wavelength regimes (e.g., Done & Gierliński 2005; Körtling, Falcke, & Corbel 2006), when compared to the predictions of RIAF models.

Understanding the quiescent BH stage is important for a variety of reasons. It is not known what triggers the active stage of luminous AGNs, with galaxy interactions, or tidal disruption and accretion of stars being favorite contenders (e.g., Volonteri et al. 2006), and details about the quiescent stage could provide clues. The existence of the BH-bulge correlations and results of galaxy-formation simulations have led to proposals that AGNs provide “feedback” that can regulate star formation and can affect galactic structure (e.g., Springel et al. 2005; Silk 2005). These ideas have been reinforced by the recent discovery of large cavities of hot gas that have been formed in the intracluster medium by jets from the nuclei of central cluster galaxies (e.g., Dunn & Fabian 2006; Nusser et al. 2006). This feedback could well take place mainly during the quiescent stage of BH activity (e.g., Heinz et al. 2007).

The low-level nuclear activity of the quiescent stage can manifest itself observationally in the form of compact, often-variable, sources of radio, UV, or X-ray emission, or as emission-line nuclei with line ratios uncharacteristic of stellar excitation, or with broad Balmer lines reminiscent of Seyfert 1 spectra (see below). Jets, generally seen in radio, but sometimes in other bands as well (e.g., as in M87) are another unambiguous indicator of nuclear activity seen in some galaxies. The weakness of these radiative signals from quiescent BHs make their study difficult, almost by definition. Problems include confusion with brighter, non-AGN,

components, obscuration by dust, and selection effects. Fortunately, it is becoming clear that a large fraction of all galactic nuclei do show some weak signs of activity that can be associated with the central BH, and in this sense most galaxies can be considered to host a low-luminosity AGN. The ubiquity and nearness of these objects (including the one in our own Galaxy) often permits separating their weak signals from the various possible backgrounds, such as radiation from stars in the optical to the UV range, and from circumnuclear accreting binaries in X-rays. In radio, high-angular resolution can help separate between jet emission and an unresolved nuclear source that could be coming directly from the accretion flow.

Probably the most common manifestation of low-luminosity AGN appears in the form low-ionization nuclear emission-line regions (LINERs; Heckman 1980), which are detected in the nuclei of a large fraction of bright nearby galaxies (Ho et al. 1997; Kauffmann et al. 2003). As their name implies, LINERs are characterized by collisionally excited lines of neutral and singly-ionized species, indicators of the presence of hot but largely neutral gas. Theoretical studies that attempted to model LINER spectra have generally agreed that LINERs are photoionized objects. The ionizing sources could be either an AGN-like UV-to-X-ray source, or a cluster of massive stars of the right mix to produce a hard-enough spectrum (e.g., Barth & Shields 2000; Kewley et al. 2006). Although the nature of LINERs and their relation, if any, to AGNs has been debated for several decades, it is now becoming clear that at least a large fraction of LINERs are indeed AGNs.¹ Kewley et al. (2006) have used Sloan Digital Sky Survey (SDSS) data to show that LINERs occupy a well-defined “cloud” in emission-line ratio diagnostic diagrams, a cloud that is distinct from the regions occupied by H II and Seyfert nuclei. This result largely overcomes previous sentiments that LINERs are a “mixed bag” of objects, with some photoionized by stars, some by AGNs, and some perhaps excited by shocks. By assuming a BH mass for every galaxy based on the BH-bulge mass relation, Kewley et al. (2006) further showed that the transition from the Seyfert region to the LINER region in the diagnostic diagrams corresponds to a decrease in the Eddington ratio, L/L_E . If this decrease is accompanied by a hardening of the ionizing spectrum, the spectral transition can also be explained.

In terms of actually detecting the ionizing continuum source in LINERs, observations at UV wavelengths, where the bright background from the bulge stellar population basically disappears, have proved to be useful. *Hubble Space Telescope* (HST) imaging showed that some 25 per cent of LINERs have compact, generally unresolved (i.e., \lesssim few pc), bright UV sources in their nuclei (Maoz et al. 1995; Barth et al. 1998). Optical HST imaging of 14 LINERs (Pogge et al. 2000) revealed that in every case where a compact UV nucleus had not been detected, obscuration of the nucleus by circumnuclear dust was apparent. This strongly suggests

¹ I will use the term LINERs here to denote only the population of compact nuclei with such emission, and will ignore a population of “extended LINERs” in which a LINER spectrum is produced under apparently different circumstances. See Sturm et al. (2006) for some recent characterizations of extended LINERs, which are relatively luminous in IR bands, and distinct in several ways from the compact sources under discussion here.

that most nearby LINERs (including the 75 per cent that are “UV-dark”, i.e., those that do not reveal a nuclear UV source at HST sensitivity, $\sim 10^{-17}$ erg cm $^{-2}$ s $^{-1}$ Å $^{-1}$) likely have such a nuclear UV source.

Maoz et al. (2005; M05) monitored with the HST *Advanced Camera for Surveys* (ACS) a sample of 17 compact UV LINER nuclei at 2500 Å and 3300 Å. They found that all but three of the objects varied in UV brightness on month-long time-scales, correlated between both UV bands, or on decade-long time-scales (by comparison to flux levels measured previously [1993–2000] for these objects at band-passes similar to the ACS 2500 Å band, usually at 2300 Å), or both. Months-scale variation amplitudes were typically ~ 10 per cent, while decadal variations were by a factor of a few. This result argues for a nonstellar UV source and, by extension to the ionizing far-UV range, for AGN excitation of the LINER emission lines. The variable UV flux provides a lower limit on the nonstellar contribution to the UV luminosity of each object.

In the radio, at Very Large Array (VLA) resolution ($0''.1 \approx$ tens of pc), about half of LINERs display unresolved radio cores at 2 cm and 3.6 cm (Nagar et al. 2000, 2002). With Very Long Baseline Interferometer (VLBI) resolution at 6 cm (~ 1 pc), these cores remain unresolved, strongly arguing for the presence of an AGN (Falcke & Biermann 1999; Falcke et al. 2000). The radio core fluxes have been found to be variable by factors of up to a few in about half of the ~ 10 LINERs observed multiple times over 3 years (Nagar et al. 2002).

At X-ray energies, *Rosat* HRI images showed compact ($< 5''$) soft X-ray emission in 70 per cent of LINERs and Seyferts (Roberts & Warwick 2000) which, when observed with *ASCA*, were found to have a nonthermal 2–10 keV spectrum (e.g., Terashima et al. 2000). Arcsecond-resolution *Chandra* observations by Terashima & Wilson (2003) of 11 LINERs, each of which was preselected to have a radio core, revealed an X-ray nucleus in all but one case, and the nuclei were generally (but not always) unresolved. Most recently, Flohic et al. (2006) found an X-ray nucleus in 12 out of 19 LINERs observed with *Chandra*. They argued that, in most cases, the observed X-ray AGN is not luminous enough to power the H α emission through photoionization. However, this conclusion depends on the assumed extrapolation of the 0.5–10 keV spectrum to far-UV energies. In fact, Flohic et al. showed that the LINERs are consistent with the best-fitting relation found by Ho et al. (2001) between 2–10 keV and H α luminosities for quasars and Seyfert 1 galaxies. This implies that, if LINERs and luminous AGNs have similar UV-to-X-ray SEDs, then there is no photoionization energy budget problem in LINERs.

The identification of the nonstellar emission components in LINERs permits obtaining a picture of the nuclear SEDs of low-luminosity AGNs across the electromagnetic spectrum. Comparison of the SEDs to theoretical predictions for different accretion modes may be the most promising avenue for understanding how BHs “sleep”.

Ho (1999) compiled and studied SEDs for seven low-luminosity AGNs, including four LINERs, a Seyfert, and two borderline LINER-Seyfert cases (in the new classification scheme of Kewley et al. [2006], both borderline cases, M81 and NGC 4579, are unambiguous LINERs). His main conclusion was that low-luminosity AGN SEDs are markedly

different from those of luminous AGNs, in that underluminous objects have a weak or absent big blue bump, and are “radio loud” in terms of the ratio of luminosity in the radio relative to other bands. However, several problems could cast doubt on these conclusions. In two of the objects (NGC 4261 and NGC 4374) the nucleus is obscured in the UV by conspicuous patches of circumnuclear dust, resulting in non-detections in this band. In a third object, NGC 6251, there are no space-UV data. Thus, only a small sample of four objects with useful measurements remain in the critical space-UV region. Ho (1999) included HST optical-band measurements in his SEDs. I will argue that this is risky because, even at HST resolutions, nuclear starlight from the centrally peaked, often cusped, bulge light distributions can dominate and therefore distort the SED in optical bands.

Ho (2002) studied further the radio-loudness issue, and showed that radio loudness anticorrelates strongly with Eddington ratio. The ratio of radio to optical luminosity in AGN samples, as a function of Eddington ratio, was recently studied also by Chiaberge et al. (2005) and Sikora et al. (2007). Both of these studies were again based on optical measurements of low-luminosity nuclear fluxes, which are susceptible to contamination by non-AGN components, even at HST resolution. The sample of Chiaberge et al. (2005) included 21 LINERs, and that of Sikora et al. (2007) has four LINER nuclei.

The SEDs of several low-luminosity AGNs have been compiled and analysed also on an individual basis: M81 and NGC 4579 (Quataert et al. 1999); NGC 6166 (Di Matteo et al. 2001); NGC 4258 (Yuan et al. 2002); IC 4296 and NGC 1399 (Pellegrini et al. 2003a); M87 (Wilson & Yang 2002; Di Matteo et al. 2003); NGC 4594 (Pellegrini et al. 2003b); NGC 3998 (Ptak et al. 2004); and NGC 4565 (Chiaberge et al. 2006). Most of these analyses did not include UV data, and sometimes did include optical and IR data, which involve the risks mentioned above. Five of these objects will be re-analysed in the present work.

In this paper, I revisit the SEDs of low-luminosity AGNs, motivated by several recent developments. First, a larger sample of LINERs having accurate HST/ACS UV photometry is now available (13, as opposed to four in Ho 1999). Furthermore, the observed variable fraction of the UV flux found by M05 in these objects provides a firm lower limit on the nonstellar AGN flux. Second, high-resolution X-ray measurements with *Chandra* and *Newton XMM* exist for most of these objects, permitting better isolation of the compact central X-ray source. Finally, recent statistical studies of the spectral properties of AGNs (e.g., Steffen et al. 2006; Sikora et al. 2007; Panessa et al. 2006,2007) allow a clearer comparison of SEDs as a function of luminosity and Eddington ratio, and thus give a better view of low-luminosity AGNs in the greater AGN context.

2 SAMPLE

My objective in this work is to investigate the luminosity ratios between radio, UV, and X-ray emission in low-luminosity LINER-type AGNs. High-angular-resolution UV measurements, possible only with HST, have been carried out for relatively few galaxies, and in only 25 per cent of the LINERs among them is the UV nucleus unobscured by

circumnuclear dust (see §1, above). I therefore start with the 17 galaxies with known central UV nuclei, monitored in 2002–2003 with HST by M05. Although originally selected by M05 as LINERs, three of the 17 objects in the M05 sample were classified by Ho et al. (1997) as Seyferts, since their narrow emission line ratios $[\text{OIII}] \lambda 5007/\text{H}\beta$ were above the defining border between LINERs and Seyferts by $\sim 30 - 40$ per cent (for M81 and NGC 3486) and by a factor ~ 3 (for NGC 4258). However, in the new classification scheme proposed by Kewley et al. (2006), and which separates well LINERs from Seyferts, M81 is clearly a LINER. NGC 3486 is a Seyfert according to its $[\text{OIII}]/\text{H}\beta$ and $[\text{OI}]/\text{H}\alpha$ ratios, but is just on the LINER-Seyfert boundary in the $[\text{OIII}]/\text{H}\beta$ vs. $[\text{SII}]/\text{H}\alpha$ diagram, and is thus an ambiguous case. NGC 4258 is a Seyfert according to its $[\text{SII}]/\text{H}\alpha$ and $[\text{OI}]/\text{H}\alpha$ ratios. I will therefore consider M81 a LINER, NGC 3486 a borderline LINER/Seyfert, and NGC 4258 a Seyfert nucleus.

From this initial selection of 17 objects, I exclude from the sample the following galaxies. NGC 4258 is excluded, because, contrary to all the other objects, it is a Seyfert, rather than a LINER. Furthermore, the morphology of its nuclear region in HST images suggests that the nucleus is partly obscured by dust (Pogge et al. 2000). This suspicion is reinforced by the high absorbing column ($N_{\text{H}} \sim 10^{23} \text{ cm}^{-2}$) fitted by Pietsch & Read (2002) to their XMM-*Newton* measurements of this object. The UV flux measured by M05 therefore likely underestimates by a large factor the unabsorbed UV flux, and using it could lead to a distorted picture of the true SED. Finally, the unabsorbed nuclear 2–10 keV flux of $12 \times 10^{-12} \text{ erg cm}^{-2} \text{ s}^{-1}$, found by Pietsch & Read (2002) corresponds to a luminosity of $\sim 10^{42} \text{ ergs s}^{-1}$, typical of Seyfert nuclei, but 100 times larger than the typical luminosities of the rest of the LINER sample. NGC 6500 is excluded because it has no clear nuclear UV source, and the nucleus may be obscured (see M05); and NGC 4569 and NGC 5055 are excluded because, for both of these cases, there are multiple lines of evidence that a young nuclear star cluster, rather than an AGN, dominates the energetics: nondetection in radio (Nagar et al. 2000); a resolved UV source (Barth et al. 1998; M05); a UV spectrum dominated by clear signatures of massive stars (Maoz et al. 1998); non-variability in the UV on both long and short time-scales (M05); and a very low X-ray luminosity (Ho et al. 2001; Flohic et al. 2006).

The remaining 13 objects in the sample include both LINERs having broad $\text{H}\alpha$ wings (which I will designate “LINER 1s”), and those having only narrow emission lines (“LINER 2s”)² The nucleus of NGC 4552, has broad components in both the permitted and the forbidden lines (Capellari et al. 1999), and therefore does not fall easily into either the type-1 or type-2 category. All but one of the 13 objects, were found to be UV-variable by M05, on short or long time-scales, or both (the exception is NGC 3486). Both types, LINER 1s and LINER 2s, are variable. M05 found a rough trend in UV colour, in the sense that LINER 2s

² Ho et al. (1997) designated LINERs with broad $\text{H}\alpha$ wings as LINER 1.9 objects. Since this is the only kind of type-1 LINER in the sample of Ho et al. (i.e., there are no known examples of LINER 1.2, 1.5, etc.), I will simply refer to LINER 1.9s as LINER 1s.

have a redder flux ratio, $f_{\lambda}(250\text{W})/f_{\lambda}(330\text{W})$, compared to LINER 1s, by a factor of ~ 2 . Table 1 lists the objects in the sample and summarizes some of their properties.

3 DATA COMPILATION

In my analysis, I will use only radio, UV, and X-ray data, and will ignore optical and IR measurements. Although high-resolution HST optical and *Spitzer* IR measurements are available for several of the LINERs in the sample, contamination by starlight, or by circumnuclear dust heated by stars, could distort the SED of the central accreting structure. Only a measurement of *variable* optical and IR flux, that could therefore be associated unambiguously with an AGN, may provide in the future useful data for this kind of analysis.

I describe below some general characteristics and considerations for selecting the data used in every band. I then relate the details of the data sources and their choices for each object individually. The data adopted for every galaxy are summarized in Table 1. I do not cite the formal measurement errors reported by the original workers. In my subsequent analysis of LINER SEDS, these errors are largely irrelevant, as they are dwarfed by bigger, systematic, errors: non-simultaneity of the measurements in the presence of variability (see below); angular resolution effects in radio bands, leading to the “resolving out” of flux at high resolutions (see, e.g., Best et al. 2005); uncertain corrections for internal extinction in the UV; and, in X-rays, uncertain absorption corrections, uncertainties in multi-component spectral modeling, and calibration uncertainties.

3.1 Radio Data

Very Large Baseline Array (VLBA) and VLBI imaging has shown that at least some of the radio emission in LINERs is contributed by jets, rather than by an actual accretion flow (e.g., Falcke et al. 2000; Nagar et al. 2002) For radio data, I have therefore searched the literature for measurements with the highest angular resolution, preferably obtained with the VLBA or the VLBI. Based on multifrequency VLBA observations of some low-luminosity AGNs, Anderson et al. (2004) have shown that, even for the unresolved milli-arcsecond core, the spectra, luminosity, and size limits are consistent with emission from jets. The observed radio flux must therefore constitute only an upper limit on the radio emission from the accretion flow itself.

3.2 UV Data

By construction, all the objects in the sample have UV measurements obtained with HST by M05, using the ACS in its High Resolution Camera (HRC) mode. M05 imaged each target in the F250W band ($\lambda_{\text{central}} \approx 2500 \text{ \AA}$, $\text{FWHM} \approx 550 \text{ \AA}$) and in the F330W band ($\lambda_{\text{central}} \approx 3300 \text{ \AA}$, $\text{FWHM} \approx 400 \text{ \AA}$). Between July 2002 and July 2003, 11 of the 13 LINERs were observed from two to five times each. Two objects, NGC 404 and NGC 1052, were observed only once. As shown by M05, the image morphologies in all 13 objects are characterized by isolated, unresolved, nuclear UV

Object	L	D Mpc	A_B mag	M_{BH}	f_ν 6 cm	f_ν 3.6 cm	f_ν 2 cm	f_ν 0.7 cm	$f_{\lambda 1.1}$ 3300 Å	f_λ 3300 Å	$f_{\lambda 1.1}$ 2500 Å	f_λ 2500 Å	f 0.5–2 keV	f 2–10 keV	Γ
(1)	(2)	(3)	(4)	(5)	(6)	(7)	(8)	(9)	(10)	(11)	(12)	(13)	(14)	(15)	(16)
NGC 404	2	3.0	0.253	5.3	...	<0.3	<0.4	<3.0	...	85.0	>41.0	134.0	1.5	...	1.8
NGC 1052	1	18.0	0.114	8.1	2410.0	2390.0	2090.0	...	670.0	9.0	>7.3	15	...	240.0	1.4
M81	1	3.6	0.346	7.8	...	132.0	165.0	...	>14.0	130.0	>16.0	200.0	...	1000.0	1.8
NGC 3368	2	10.7	0.109	7.4	<0.6	30.0	>17.0	22.0	...	16.0	1.8
NGC 3486	2	7.4	0.093	6.2	<0.1	18.2	...	10.8	...	<0.5	1.8
NGC 3642	1	27.5	0.046	7.1	<0.4	...	>1.8	22.1	>2.0	24.5	26.0	...	1.8
NGC 3998	1	13.1	0.069	8.4	83.0	>28.0	153.0	>38.0	199.0	...	1100.0	1.9
NGC 4203	1	15.1	0.052	7.0	8.1	8.5	10.2	9.9	>13.0	37.0	>57.0	58.0	119.0	125.0	1.8
M87	2	15.4	0.096	9.5	3000.0	48.0	>45.0	100.0	59.0	...	2.2
NGC 4552	?	15.4	0.177	8.5	99.5	...	59.0	...	>0.3	1.5	>0.4	2.0	5.0	6.0	1.8
NGC 4579	1	21.0	0.177	7.8	19.2	16.2	15.3	14.6	>2.9	42.0	>77.0	110.0	300.0	380.0	1.7
NGC 4594	2	9.1	0.120	9.0	123.0	...	100.0	...	>1.7	15.3	>5.1	12.0	55.0	130.0	1.9
NGC 4736	2	4.9	0.076	7.1	...	1.7	1.7	73.0	>2.0	39.0	...	27.0	1.6

Table 1. Adopted Data. See §3 for sources and references for all data. Column header explanations: (2)- Type-1 or type-2 LINER, depending on presence or absence, respectively, of broad H α . NGC 4552, which does not fall easily into either category (see text), is marked with a “?”; (3) - distance (4) - B -band Galactic extinction; (5) - log of black hole mass, in Solar-mass units; (6)-(9) - monochromatic radio flux per unit frequency, in mJy. upper limits are 3σ ; (10)-(13) - monochromatic UV flux per unit wavelength, in units of $10^{-17}\text{erg cm}^{-2}\text{s}^{-1}\text{\AA}^{-1}$. Columns headed “1.1.” give a lower limit on the nontellar contribution based on the variable flux; (14)-(15) absorption-corrected X-ray flux, in units of $10^{-14}\text{erg cm}^{-2}\text{s}^{-1}$; (16)- X-ray photon index. When unknown, $\Gamma = 1.8$ is assumed.

sources, facilitating the photometric measurements. As described in detail in M05, ACS/HRC photometry is very stable, with a photometric rms scatter of less than 1 per cent in both the F250W and the F330W bands.

The M05 data permit extracting several measures of UV flux. The variable UV flux provides a firm lower limit to the intrinsic, unextinguished, AGN UV flux. However, the highest observed flux, to which I will refer as the “high flux”, is also interesting; its non-variable fraction could be mainly or wholly from the AGN as well, but simply did not happen to vary during the M05 monitoring campaign. If there is some internal extinction by dust, the actual flux could be even higher. On the other hand, some or all of the non-variable fraction could be due to massive stars, and could undergo little or no extinction, in which case the high flux would be an overestimate of the AGN flux.

In addition to the M05 data, I consider both the absolute and variable UV fluxes of each object based on previous UV observations with HST, as discussed below individually for each object. Most of these previous data are at $\sim 2300\text{\AA}$, which for the present purposes I will consider close enough in wavelength to be equivalent to the 2500\AA measurements of M05.

3.3 X-ray Data

X-ray data were compiled for most of the sample based on observations with *Chandra* and/or *Newton-XMM*, which have angular resolutions of $\sim 1''$. In a few cases, even though such data exist, the nuclear sources are too bright to be measured reliably by *Chandra*, due to “pile-up” in its detectors. In these cases, measurements from older satellites are used, after considering the evidence for the influence of non-nuclear sources on the measured flux. When X-ray power-law photon spectral indices are not available, I will assume a typical low-luminosity photon index of $\Gamma = 1.8$ (e.g., Ho et al. 2001), where the photon flux per energy interval, $d\epsilon$, is $dN/d\epsilon \propto \epsilon^{-\Gamma}$.

3.4 Distances

I will describe the SEDs of the AGNs in the sample in terms of their luminosities in the different bands, as calculated using an assumed distance to each galaxy. My analysis of interband luminosity ratios will not depend on the assumed distances, but accurate distances can be important in some SED studies (e.g., errors in distances can produce an artificial correlation between luminosities in different bands). I adopt the recent distance measurements to the sample galaxies compiled from the literature by M05. In 11/13 cases (the exceptions are NGC 3486 and NGC 3642), the distances are based on “modern” methods – Cepheids, surface-brightness fluctuations, tip of the red giant branch, and Tully-Fisher.

3.5 Black Hole Masses

Four of the objects in the sample (M81, NGC 3998, M87, and NGC 4594) have in the literature measured BH masses based on stellar or gas kinematics, which I adopt. In most of the remaining cases, I estimate BH masses using the Tremaine et al. (2002) mass vs. velocity-dispersion relation, using stellar velocity dispersion measurements taken from the Hyperleda database³. An exception is NGC 4203, for which the Tremaine et al. (2002) relation predicts a BH mass of $6.6 \times 10^7 M_\odot$, but for which Sarzi et al. (2002) set a 1σ upper limit of $2.4 \times 10^7 M_\odot$. In this case I assume a mass of $1 \times 10^7 M_\odot$.

3.6 Individual Objects

NGC 404 – Nagar et al. (2000) did not detect a radio core with the VLA in this galaxy at wavelengths of 0.7, 2, and 3.6 cm, to 3σ limits of 3 mJy, 0.39 mJy, and 0.27 mJy, respectively.

HST UV spectroscopy of the compact nucleus by Maoz et al. (1998) showed clear absorption signatures of

³ <http://leda.univ-lyon1.fr>

OB stars, contributing at least 40 per cent of the UV light. However, the relative shallowness of the absorptions meant that the light from massive stars was diluted by another component, comparable in flux, which could be a featureless AGN continuum, or the light from less massive stars in an aging or continuous starburst. In the single epoch of HST/ACS data by M05, the 2500 Å flux ($74 \times 10^{-17} \text{ erg cm}^{-2} \text{ s}^{-1} \text{ \AA}^{-1}$) was ≈ 60 per cent of the level measured by the 1994 spectroscopy analysed by Maoz et al. (1998; $115 \times 10^{-17} \text{ erg cm}^{-2} \text{ s}^{-1} \text{ \AA}^{-1}$), and only 45 per cent of the HST Faint Object Camera (FOC) imaging measurement in 1993 by Maoz et al. (1995; $180 \times 10^{-17} \text{ erg cm}^{-2} \text{ s}^{-1} \text{ \AA}^{-1}$ at 2300 Å). I will therefore adopt a lower limit on the non-stellar 2500 Å flux, of $(115 - 74) \times 10^{-17} \text{ erg cm}^{-2} \text{ s}^{-1} \text{ \AA}^{-1}$. At 2300 Å, the AGN flux may have been as high as the level measured in 1993, minus the minimum stellar contribution, or approximately $(180 - 0.4 \times 115) \times 10^{-17} \text{ erg cm}^{-2} \text{ s}^{-1} \text{ \AA}^{-1}$, which I will adopt as the “high flux” for this object. At 3300 Å, M05 measured a flux of $85 \times 10^{-17} \text{ erg cm}^{-2} \text{ s}^{-1} \text{ \AA}^{-1}$,

In X-rays, a *Chandra* measurement of the compact nuclear source by Eracleous et al. (2002) gives an 0.5–2 keV flux of $1.5 \times 10^{-14} \text{ erg cm}^{-2} \text{ s}^{-1}$.

NGC 1052 – Kadler et al. (2004) have used VLBA to resolve the core into milliarcsecond-scale twin jets, with a total flux at 0.7, 3.6, and 6 cm, of 670 mJy, 2390 mJy, and 2410 mJy, respectively. There is a small gap between the jets, and it is not clear which component, if any, can be associated directly with the nucleus.

In the single epoch measured by M05 in 2002, the UV flux was $7.7 \times 10^{-17} \text{ erg cm}^{-2} \text{ s}^{-1} \text{ \AA}^{-1}$ at 2500 Å and $9.0 \times 10^{-17} \text{ erg cm}^{-2} \text{ s}^{-1} \text{ \AA}^{-1}$ at 3300 Å. The short wavelength flux was at half the level of the 2300 Å flux in a 1997 HST Faint Object Spectrograph (FOS) spectrum (Gabel et al. 2000), as measured by Pogge et al. (2000; $15 \times 10^{-17} \text{ erg cm}^{-2} \text{ s}^{-1} \text{ \AA}^{-1}$), which I will adopt as a high flux. Based on the variable fraction, the lower limit on the AGN flux is then $(15 - 7.7) \times 10^{-17} \text{ erg cm}^{-2} \text{ s}^{-1} \text{ \AA}^{-1}$.

Kadler et al. (2004) have used *Chandra* to measure an unabsorbed nuclear 0.2–8 keV flux of $300 \times 10^{-14} \text{ erg cm}^{-2} \text{ s}^{-1}$. They find the X-rays are moderately absorbed by a column density of $\sim 10^{22} \text{ cm}^{-2}$. The photon index they derive, $\Gamma = 0.3$, is extremely low, but they note that this could be the result of pile-up in the detector at low energies. I therefore adopt the photon index of $\Gamma = 1.4$ obtained by Guainazzi et al. (2000) using *BeppoSAX*. For this index, the 2–10 keV flux would be $240 \times 10^{-14} \text{ erg cm}^{-2} \text{ s}^{-1}$

M81 (NGC 3031) – Bietenholz et al. (2000) used VLBI to measure in this galaxy a radio core with 132 mJy at 3.6 cm, and Nagar et al. (2002) obtained 165 mJy at 2 cm with the VLBA.

M81 was imaged by M05 at five epochs. The mean level at 2500 Å, $200 \times 10^{-17} \text{ erg cm}^{-2} \text{ s}^{-1} \text{ \AA}^{-1}$, was similar to the one measured by Maoz et al. (1998) at 1500 Å in the 1993 HST/FOS spectrum of Ho et al. (1996) – $150 \times 10^{-17} \text{ erg cm}^{-2} \text{ s}^{-1} \text{ \AA}^{-1}$. [From an analysis of the FOS target acquisition records, Maoz et al. (1998) deduced that M81 was located at the edges of its peak-up scans, possibly leading to some light loss.] The flux level measured by M05 is also the same as the 2200 Å flux estimated by Maoz et al. (1998) by extrapolating the 1996 WFPC2 measurement at $\sim 1600 \text{ \AA}$ by Devereux et al. (1997). The mean 3300 Å flux

found by M05 was $130 \times 0.11 \times 10^{-17} \text{ erg cm}^{-2} \text{ s}^{-1} \text{ \AA}^{-1}$. Variations measured by M05 in both F250W (8 per cent) and F330W (11 per cent) give a lower limits on the AGN flux of $200 \times 0.08 \times 10^{-17} \text{ erg cm}^{-2} \text{ s}^{-1} \text{ \AA}^{-1}$, and $130 \times 0.11 \times 10^{-17} \text{ erg cm}^{-2} \text{ s}^{-1} \text{ \AA}^{-1}$, respectively.

Ho et al. (2001) measured with *Chandra* an unabsorbed 2–10 keV flux from the nucleus of $1.0 \times 10^{-11} \text{ erg cm}^{-2} \text{ s}^{-1}$. Because the nuclear source was heavily piled up, the counts were estimated from the readout trail.

A central BH mass of $6 \times 10^7 M_{\odot}$ has been reported by Bower et al. (2000) based on stellar kinematics, and $7 \times 10^7 M_{\odot}$ by Devereux et al. (2003) based on gas kinematics. I adopt the mean of the two.

NGC 3368 – Nagar et al. (2000) report a 3σ limit of 0.6 mJy at 2 cm on any radio core at VLA resolution ($\sim 1''$).

M05 found no UV variations between the two epochs, in 2002 and 2003, at which this LINER 2 was observed. However, the 2500 Å flux ($22 \times 10^{-17} \text{ erg cm}^{-2} \text{ s}^{-1} \text{ \AA}^{-1}$) was a factor of 4.5 higher than the 2300 Å flux measured in 1993 with HST/FOC by Maoz et al. (1996; $5 \times 10^{-17} \text{ erg cm}^{-2} \text{ s}^{-1} \text{ \AA}^{-1}$). The variable fraction gives a lower limit on the AGN flux of $(22 - 5) \times 10^{-17} \text{ erg cm}^{-2} \text{ s}^{-1} \text{ \AA}^{-1}$. For the high flux, I adopt $22 \times 10^{-17} \text{ erg cm}^{-2} \text{ s}^{-1} \text{ \AA}^{-1}$ at 2500 Å and $30 \times 10^{-17} \text{ erg cm}^{-2} \text{ s}^{-1} \text{ \AA}^{-1}$ at 3300 Å.

In X-rays, Satyapal et al. (2004) used *Chandra* to measure a 2–10 keV flux of $16 \times 10^{-14} \text{ erg cm}^{-2} \text{ s}^{-1}$.

NGC 3486 – In this borderline Seyfert/LINER nucleus, no radio cores at 6 cm and 20 cm were detected at a VLA resolution of $1''$ by Ho & Ulvestad (2001), to a 3σ limit of $0.12 \text{ mJy beam}^{-1}$.

In the UV monitoring by M05, this source displayed neither short-term changes between the two, closely spaced (by 1 month), epochs in which it was observed, nor long-term variations when comparing the 2500 Å flux to a 2300 Å measurement in 1993 with the HST/FOC by Maoz et al. (1996). The 2500 Å and 3300 Å flux levels are $10.8 \times 10^{-17} \text{ erg cm}^{-2} \text{ s}^{-1} \text{ \AA}^{-1}$, and $18.2 \times 10^{-17} \text{ erg cm}^{-2} \text{ s}^{-1} \text{ \AA}^{-1}$, respectively. Thus, there is no variability-based lower limit on the AGN flux in this object.

Ho et al. (2001) used *Chandra* to set an upper limit of $0.5 \times 10^{-14} \text{ erg cm}^{-2} \text{ s}^{-1}$ on the 2–10 keV nuclear flux.

Given the X-ray and radio non-detections and the UV non-variability, M05 discussed the possibility that this is another non-AGN LINER with UV emission dominated by stars, like NGC 4569 and NGC 5055, which I have excluded from the present sample for this reason. M05 noted, however, that M81 and M87, which are clearly AGNs with variable UV flux, were also near their “historical” UV levels in the M05 campaign, and were constant in the two closely spaced epochs (for M87) or in four out of five epochs (for M81). Thus, detection of short-term variability in NGC 3486 might have been possible with better temporal sampling. I will therefore keep NGC 3486 in the sample, allowing for the possibility that its UV flux is AGN dominated.

NGC 3642 – Nagar et al. (2000) placed a 3σ upper limit of 0.39 mJy on the 2 cm radio flux from this nucleus, at VLA resolution.

M05 measured 8 per cent peak-to-peak amplitude variations around the mean 2500 Å level, $24.5 \times 10^{-17} \text{ erg cm}^{-2} \text{ s}^{-1} \text{ \AA}^{-1}$, providing a lower limit on the AGN flux. The 3300 Å flux was $22.1 \times$

$10^{-17} \text{ erg cm}^{-2} \text{ s}^{-1} \text{ \AA}^{-1}$), but not definitively variable. The 30 per cent increase in 2500 Å flux compared to the 2300 Å WFPC2 measurement in 1994 by Barth et al. (1998; $19 \times 10^{-17} \text{ erg cm}^{-2} \text{ s}^{-1} \text{ \AA}^{-1}$) was not deemed large enough to be considered significant, given the different bandpasses and the UV sensitivity fluctuations of WFPC2.

A *Rosat*-HRI measurement by Koratkar et al. (1995) shows that the nuclear X-ray emission is concentrated within $\lesssim 5''$. Using the *ROSAT*-PSPC, Komossa et al. (1999) measured for this source a 1-2.4 keV flux of $18 \times 10^{-14} \text{ erg cm}^{-2} \text{ s}^{-1}$. For an assumed photon index of $\Gamma = 1.8$, this would correspond to a 0.5–2 keV flux of $26 \times 10^{-14} \text{ erg cm}^{-2} \text{ s}^{-1}$.

NGC 3998 – In this nucleus, Filho et al. (2002) have measured a variable radio core that is unresolved at 5 mas resolution with VLBI, with a mean 6 cm flux of 83 mJy.

In the UV, M05 measured in 2002–2003 a monotonic 20 per cent decline in UV flux in the F250W and F330W bands (means of $199 \times 10^{-17} \text{ erg cm}^{-2} \text{ s}^{-1} \text{ \AA}^{-1}$ and $153 \times 10^{-17} \text{ erg cm}^{-2} \text{ s}^{-1} \text{ \AA}^{-1}$, respectively), over the 11 months they observed it. These variations provide firm lower limits on the AGN flux. On long time-scales, the mean 2500 Å flux level in 2003 was about 5 times lower than reported by Fabbiano et al. (1994; $10^{-14} \text{ erg cm}^{-2} \text{ s}^{-1} \text{ \AA}^{-1}$) at 1740 Å in 1992, based on FOC measurements. There is thus evidence for a large variable UV flux, of order $10^{-14} \text{ erg cm}^{-2} \text{ s}^{-1} \text{ \AA}^{-1}$. However, because of the different UV band, I will not adopt the Fabbiano et al. (1994) point as a lower limit, and conservatively use only the variable flux measured by M05. Ptak et al. (2004) used the Optical Monitor on *XMM-Newton* to roughly estimate a 2100 Å UV flux of $250 \text{ to } 500 \times 10^{-17} \text{ erg cm}^{-2} \text{ s}^{-1} \text{ \AA}^{-1}$ in 2001, intermediate to the 1992 and 2003 levels.

The X-ray flux found by Ptak et al. (2004) using *XMM-Newton* is $1100 \times 10^{-14} \text{ erg cm}^{-2} \text{ s}^{-1}$ at 2–10 keV, and is consistent with, though perhaps a factor of ~ 2 higher than, previous X-ray measurements over the past two decades. The photon index is $\Gamma = 1.9$.

A central BH mass of $2.7 \times 10^8 M_\odot$ has been measured by de Francesco et al. (2006) using gas kinematics.

NGC 4203 – VLBA measurements by Anderson et al. (2004) of the unresolved (at the mas scale) core provide the following fluxes: 9.9 mJy at 0.7 cm; 9.0 mJy at 1.35 cm; 10.2 mJy at 1.9 cm; 8.5 mJy at 3.6 cm; 8.1 mJy at 6 cm. Nagar et al. (2002) have found that the radio core is variable.

In the UV monitoring by M05, the nuclear source showed large fluctuations, 1.5 between maximum and minimum in F250W (mean: $58 \times 10^{-17} \text{ erg cm}^{-2} \text{ s}^{-1} \text{ \AA}^{-1}$), and 1.4 in F330W (mean: $37 \times 10^{-17} \text{ erg cm}^{-2} \text{ s}^{-1} \text{ \AA}^{-1}$). The 2500 Å flux level in 2003 was 3-4 times higher than in the HST/WFPC2 2300 Å measurement by Barth et al. (1998; $21 \times 10^{-17} \text{ erg cm}^{-2} \text{ s}^{-1} \text{ \AA}^{-1}$), obtained in 1994. The variable UV flux, which provides a lower limit on the AGN component, is thus $13 \times 10^{-17} \text{ erg cm}^{-2} \text{ s}^{-1} \text{ \AA}^{-1}$ at 3300 Å, and $(78 - 21) \times 10^{-17} \text{ erg cm}^{-2} \text{ s}^{-1} \text{ \AA}^{-1}$ at 2500 Å.

Ho et al. (2001) measured with *Chandra* a 2–10 keV flux of $44 \times 10^{-14} \text{ erg cm}^{-2} \text{ s}^{-1}$. Terashima et al. (2002) measured with *ASCA* a flux of $119 \times 10^{-14} \text{ erg cm}^{-2} \text{ s}^{-1}$ at 0.5–2 keV, $205 \times 10^{-14} \text{ erg cm}^{-2} \text{ s}^{-1}$ at 2–10 keV, and a photon index $\Gamma = 1.8$. Terashima & Wilson (2003) verified that, although source was too bright to be measured with *Chandra*,

the nuclear source is unresolved and dominates the emission at the *ASCA* spatial resolution. I will adopt at 0.5–2 keV the *ASCA* measurement, and at 2–10 keV the mean of the *ASCA* and *Chandra* measurements, $125 \times 10^{-14} \text{ erg cm}^{-2} \text{ s}^{-1}$, with a photon index $\Gamma = 1.8$.

As noted above, the Tremaine et al. (2002) relation predicts, given the velocity dispersion in this galaxy, 167 km s^{-1} , a BH mass of $6.6 \times 10^7 M_\odot$, but Sarzi et al. (2002) set an upper limit of $2.4 \times 10^7 M_\odot$. In this case I will therefore assume a mass of $1 \times 10^7 M_\odot$.

M87 (NGC 4486) – A 2 cm VLBA measurement of the unresolved core of M87 by Kellerman et al. (2004), with 1 mas resolution, is 3 Jy, consistent with a VLA (1'' resolution) measurement by Biretta et al. (1991).

The UV flux is variable on short time-scales (Perlman et al. 2003; M05) as well as on long ones (M05). At 2500 Å, I will adopt a high flux of $100 \times 10^{-17} \text{ erg cm}^{-2} \text{ s}^{-1} \text{ \AA}^{-1}$, based on an HST/FOC measurement by Maoz et al. (1996). A lower limit of the nonstellar AGN flux in the UV is obtained from the difference between this measurement and that of M05, $(100 - 55) \times 10^{-17} \text{ erg cm}^{-2} \text{ s}^{-1} \text{ \AA}^{-1}$. At 3300 Å, M05 found $48 \times 10^{-17} \text{ erg cm}^{-2} \text{ s}^{-1} \text{ \AA}^{-1}$, and little variability between their two, closely spaced, epochs.

In X-rays, Wilson and Yang (2002) measured with *Chandra* a flux density at 1 keV of $37 \times 10^{-14} \text{ erg cm}^{-2} \text{ s}^{-1} \text{ keV}^{-1}$. Di Matteo et al. (2003) found, using the same data, $(80 \pm 2) \times 10^{-14} \text{ erg cm}^{-2} \text{ s}^{-1} \text{ keV}^{-1}$. I will adopt the mean of these two observations, $59 \times 10^{-14} \text{ erg cm}^{-2} \text{ s}^{-1} \text{ keV}^{-1}$. Both analyses find a photon index of $\Gamma = 2.2$

A central BH mass of $3.4 \times 10^9 M_\odot$ has been measured by Macchetto et al. (1997) using gas kinematics.

NGC 4552 – Nagar et al. (2002) measured with the VLBA at 6 cm (2 mas resolution) a flux 99.5 mJy, and with the VLA at 2 cm (150 mas resolution) a flux of 59 mJy

The various UV measurements of this nucleus with HST are: $1.5 \times 10^{-17} \text{ erg cm}^{-2} \text{ s}^{-1} \text{ \AA}^{-1}$ (at 2300 Å) and $1.8 \times 10^{-17} \text{ erg cm}^{-2} \text{ s}^{-1} \text{ \AA}^{-1}$ (at 2800 Å), with HST/FOC in 1993 (Cappellari et al. 1999); $2 \times 10^{-17} \text{ erg cm}^{-2} \text{ s}^{-1} \text{ \AA}^{-1}$ at 2500 Å with HST/FOS in 1996 (Cappellari et al. 1999); M05 observed it at two epochs between which it brightened by 20 per cent in both F250W and F330W. I adopt the means of the measurements of M05, $2 \times 10^{-17} \text{ erg cm}^{-2} \text{ s}^{-1} \text{ \AA}^{-1}$ (F250W), and $1.5 \times 10^{-17} \text{ erg cm}^{-2} \text{ s}^{-1} \text{ \AA}^{-1}$ (F330W), and take 20 per cent of them as lower limits on the AGN flux.

Flohic et al. (2006) used *Chandra* to derive unabsorbed fluxes for the nuclear source of $5.0 \times 10^{-14} \text{ erg cm}^{-2} \text{ s}^{-1}$ at 0.5–2 KeV, and $6.0 \times 10^{-14} \text{ erg cm}^{-2} \text{ s}^{-1}$ at 2–10 KeV, and a photon index of 2.0 ± 0.2 . Machacek et al. (2006) find a photon index of 1.7, and I will adopt a value of 1.8.

NGC 4579 – VLBA measurements by Anderson et al. (2004) of the radio core, unresolved at 1 mas, are: 14.6 mJy at 0.7 cm; 11.1 mJy at 1.35 cm; 15.3 mJy at 1.9 cm; 16.2 mJy at 3.6 cm; 19.2 mJy at 6 cm.

The various UV fluxes that have been measured with HST, from low to high, are: at $\sim 2300 \text{ \AA}$ in 1994, $33 \times 10^{-17} \text{ erg cm}^{-2} \text{ s}^{-1} \text{ \AA}^{-1}$ (Barth et al. 1996; Maoz et al. 1998); at 2500 Å in 2003, $61 \times 10^{-17} \text{ erg cm}^{-2} \text{ s}^{-1} \text{ \AA}^{-1}$ (M05, mean of two epochs); at 3300 Å in 2003, $42 \times 10^{-17} \text{ erg cm}^{-2} \text{ s}^{-1} \text{ \AA}^{-1}$ (M05, mean of two epochs); and at $\sim 2300 \text{ \AA}$ in 1993, $110 \times 10^{-17} \text{ erg cm}^{-2} \text{ s}^{-1} \text{ \AA}^{-1}$ (Maoz et

al. 1995); Between the two epochs of M05, separated by less than a month, the nucleus brightened by 7 per cent in both UV bands. I will adopt the Maoz et al. (1995) measurement as a high point at 2500 Å, the difference between the Maoz et al. (1995) and the Maoz et al. (1998) measurements at 2200 Å as lower limits on the AGN flux, the M05 mean flux at 3300 Å as a high point, and 7 per cent of this value as the lower limit on the AGN flux at 3300 Å.

Eracleous et al. (2002) find with *Chandra* an unabsorbed 2–10 keV nuclear flux of 1300×10^{-14} erg cm⁻² s⁻¹, with a photon index of 1.8. Analysis by Cappi et al. (2006) of a measurement with *XMM-Newton* gives 300×10^{-14} erg cm⁻² s⁻¹ at 0.5–2 keV, and 380×10^{-14} erg cm⁻² s⁻¹ at 2–10 keV, with a photon index of 1.7. Since pile-up is a concern in *Chandra* data for this bright source (Terashima & Wilson 2003), I will adopt the XMM values.

NGC 4594 – The radio core flux at 6 cm measured by Hummel et al. (1984) with the VLA at 1'' resolution was 123 mJy, consistent with a VLBI measurement by Graham et al. (1981). At 2 cm, Hummel et al. (1984) measured an unresolved (< 0''.02) flux of 100 mJy.

M05 reported short-term UV variations, with 20 per cent peak-to-peak amplitude in F250W and 11 per cent in F330W, and mean UV fluxes of 7.5×10^{-17} erg cm⁻² s⁻¹ Å⁻¹ (F250W), and 15.3×10^{-17} erg cm⁻² s⁻¹ Å⁻¹ (F330W). I take as a lower limit on the 2500 Å AGN flux the difference between the level measured with the FOS in 1995 (Nicholson et al. 1998; Maoz et al. 1998) and the lowest level found by M05, $(12 - 6.9) \times 10^{-17}$ erg cm⁻² s⁻¹ Å⁻¹, and a high flux based on the FOS measurement. A lower limit at 3300 Å, based on the variability observed by M05, is $0.11 \times 15.3 \times 10^{-17}$ erg cm⁻² s⁻¹ Å⁻¹.

In X-rays, I use the *XMM-Newton* measurements by Pellegrini et al. (2003b), 55×10^{-14} erg cm⁻² s⁻¹ at 0.5–2 keV, and 130×10^{-14} erg cm⁻² s⁻¹ at 2–10 keV, with $\Gamma = 1.9$.

A central BH mass of $1 \times 10^9 M_\odot$ has been measured by Kormendy et al. (1996) using stellar kinematics.

NGC 4736 – VLA measurements with a resolution of 0''.15 reveal an unresolved nuclear source with a flux of 1.7 mJy at 2 cm (Nagar et al. 2005). At 3.5 cm, with a resolution of 0''.24, KÖrding et al. (2005) also find a flux of 1.7 mJy.

Maoz et al. (1996) used the HST/FOC in 1993 to measure a 2300 Å flux of 19×10^{-17} erg cm⁻² s⁻¹ Å⁻¹. M05 reported that, in the ACS F250W band in 2003, the nucleus was significantly brighter than in 1993, at 48×10^{-17} erg cm⁻² s⁻¹ Å⁻¹. However, reanalysis of the M05 images raises some doubts. The nuclear source in this galaxy is superimposed on a fairly bright diffuse stellar background, and the nuclear flux is sensitive to the aperture used for the measurement. Compared to the FOC F220W image, the stellar background is more prominent in the redder F250W measurement by M05 which, being a CCD observation, is also more susceptible to red leak. Photometry of the M05 data using an aperture smaller than used by M05 (and smaller than the minimum that M05 found was required to provide reliable photometry in these ACS data) gives a value closer to the 1993 level. On the other hand, the 1993 FOC data were affected by non-linearity and saturation, both of which would lead to an

underestimate of the true flux. Given these uncertainties, I will adopt the mean level between these measurements, 39×10^{-17} erg cm⁻² s⁻¹ Å⁻¹ for the 2500 Å flux, and the M05 value at 3300 Å, 73×10^{-17} erg cm⁻² s⁻¹ Å⁻¹. The UV variability amplitude during the M05 campaign was only 5 per cent at 2500 Å, and null at 3300 Å, providing a weak lower limit on the AGN flux.

In *Chandra* X-ray images obtained by Eracleous et al. (2002), the unresolved nuclear source (X-2 in their table 4) has a 2–10 keV flux of 27×10^{-14} erg cm⁻² s⁻¹ at 2–10 keV, and a photon index of 1.6.

4 DERIVED QUANTITIES

The analysis that follows will be based mainly on luminosities at 6 cm, 2500 Å, and 2 keV. The following conversions are therefore performed on the data adopted in the previous section, and listed in Table 1.

When high-angular-resolution 5 GHz fluxes are unavailable, I assume the median spectral index s ($f_\nu \propto \nu^s$, where ν is frequency, and f_ν is monochromatic flux) found by Nagar et al. (2001) for the core emission in a sample of low-luminosity AGNs, $s = -0.2$, in order to convert monochromatic fluxes from 15 GHz to 5 GHz.

I correct all UV fluxes for Galactic extinction, assuming the *B*-band extinction values (listed in Table 1) of Schlegel et al. (1998), and the Galactic extinction curve of Cardelli et al. (1989), with the parameter $R_V = 3.1$.

Monochromatic X-ray fluxes at 2 keV are recovered from the 0.5–2 KeV or 2–10 keV fluxes listed in Table 1, for the adopted power-law photon spectral indices. When photon indices are not available, I assume a typical low-luminosity photon index of $\Gamma = 1.8$ (e.g., Ho et al. 2001). When both 0.5–2 KeV and 2–10 keV fluxes are available, I use the mean of the two 2 keV monochromatic fluxes obtained.

All monochromatic fluxes, f_ν , are converted to luminosities, L_ν and νL_ν , using the adopted distances to the galaxies, listed in Table 1. Luminosities in units of the Eddington luminosity, $L_E = 1.3 \times 10^{38} (M/M_\odot)$, are obtained using the BH masses in Table 1.

The ratio of UV to X-ray luminosity in AGNs is usually discussed in terms of α_{ox} , the spectral index of a hypothetical power-law between L_ν at 2500 Å and at 2 keV, or

$$\alpha_{\text{ox}} \equiv \frac{\log[L_\nu(2500 \text{ \AA})/L_\nu(2 \text{ keV})]}{\log[(\nu(2500 \text{ \AA}))/\nu(2 \text{ keV})]} \\ = 0.384 \log[L_\nu(2 \text{ keV})/L_\nu(2500 \text{ \AA})]. \quad (1)$$

I derive two values of α_{ox} for every galaxy in the sample, one based on the ‘‘high point’’ UV flux, and one based on the lower limit on the UV flux from an AGN, based on the variable flux. The latter provides an upper limit on α_{ox} . One galaxy, NGC 3486, did not vary during the M05 campaign or before it, and hence there is no lower limit on its AGN UV flux. Furthermore, the nucleus is undetected in X-rays with only an upper limit. In this case I therefore use the UV ‘‘high point’’ and the X-ray upper limit to derive only an upper limit on α_{ox} .

‘‘Radio loudness’’, R , is usually discussed in terms of the ratio of the luminosity at 5 GHz to the luminosity in

Object	$\log(\nu L_\nu)$ 6 cm	$\log(\nu L_\nu)$ 2500 Å l.l.	$\log(\nu L_\nu)$ 2500 Å	$\log(\nu L_\nu)$ 2 keV	$\log R_{UV}$ u.l.	$\log R_{UV}$	α_{ox} u.l.	α_{ox}	$\log(\nu L_\nu/L_E)$ 2500 Å
(1)	(2)	(3)	(4)	(5)	(6)	(7)	(8)	(9)	(10)
NGC 404	< 34.44	> 39.24	39.75	37.14	< 0.59	< 0.08	< -1.81	-2.00	-3.7
NGC 1052	39.68	> 39.93	40.24	40.54	< 5.13	4.81	< -0.77	-0.89	-5.9
M81	37.21	> 39.04	40.14	39.92	< 3.55	2.45	< -0.66	-1.08	-5.8
NGC 3368	< 35.71	> 39.84	39.95	39.06	< 1.25	< 1.14	< -1.30	-1.34	-5.5
NGC 3486	< 34.60	...	39.31	< 37.24	...	< 0.66	...	-1.80	-5.0
NGC 3642	< 36.35	> 39.69	40.78	40.29	< 2.05	< 0.96	< -0.77	-1.19	-4.4
NGC 3998	37.93	> 40.34	41.06	41.12	< 2.98	2.26	< -0.70	-0.98	-5.5
NGC 4203	37.05	> 40.63	40.64	40.35	< 1.80	1.79	< -1.11	-1.11	-4.5
M87	39.73	> 40.57	40.92	40.02	< 4.54	4.19	< -1.21	-1.35	-6.7
NGC 4552	38.15	> 38.58	39.27	39.01	< 4.96	4.26	< -0.83	-1.10	-7.4
NGC 4579	37.71	> 41.13	41.29	41.07	< 1.96	1.80	< -1.02	-1.08	-4.6
NGC 4594	37.78	> 39.18	39.56	39.76	< 3.98	3.61	< -0.78	-0.92	-7.6
NGC 4736	35.48	> 38.21	39.50	38.54	< 2.66	1.37	< -0.87	-1.37	-5.7

Table 2. Derived Quantities. See §4 for details of quantity derivations. Column header explanations: (2)-(5) - \log of the luminosity, $(\nu L_\nu)/(\text{erg s}^{-1})$; (3) - lower limit of the 2500 Å luminosity, based on the variable flux in Table 1; (6)-(7) - radio loudness parameter, $R_{UV} \equiv L_\nu(6 \text{ cm})/L_\nu(2500 \text{ Å})$; (6) - upper limit on R_{UV} based on the lower limit on the 2500 Å luminosity; (8)-(9) - α_{ox} parameter, $\equiv 0.384 \log[L_\nu(2 \text{ keV})/L_\nu(2500 \text{ Å})]$; (8) - upper limit on α_{ox} based on the lower limit on the 2500 Å luminosity; (10) - \log of the 2500 Å luminosity, νL_ν , as a fraction of the Eddington luminosity, $L_E = 1.3 \times 10^{38} (M/M_\odot)$.

optical, UV, or X-ray bands. I will define R_{UV} as the ratio of L_ν between 5 GHz and 2500 Å,

$$R_{UV} \equiv L_\nu(6 \text{ cm})/L_\nu(2500 \text{ Å}). \quad (2)$$

As in the case of α_{ox} , I calculate two values of R_{UV} for each galaxy, one based on the high UV measurement in Table 1, and another based on the lower limit on the nonstellar UV flux, which gives an upper limit on R_{UV} . In three galaxies, NGC 404, NGC 3368, and NGC 3642, no radio core has been detected. The upper limit on the radio flux in each of these cases, combined with the UV high point and lower limit, give two separate upper limits on R_{UV} . In a fourth case, NGC 3486, there is an upper limit on the radio flux, and no UV variability is detected. In this case, there is only one upper limit on R_{UV} , based on the constant UV flux.

5 RESULTS

The numbers compiled and derived above permit a renewed look at the SEDs of unobscured, LINER-type, low-luminosity AGNs, particularly the ratios of their UV, X-ray, and radio luminosities. Table 2 lists the monochromatic luminosities νL_ν of every object at the various frequencies, based on the fluxes in Table 1 in the different bands, after the necessary corrections and conversions, and the main derived quantities for the sample: α_{ox} , and R_{UV} , each based on both the lower-limit UV flux and the high UV flux.

5.1 The SED

Figure 1 displays the SED data of each object, based on the data in Table 1. Following Ho (1999), I overlay in every frame the mean SEDs of radio-loud and radio-quiet quasars from Elvis et al. (1994), normalized to pass through the high UV 2500 Å measurements for the LINERs. All the multi-wavelength measurements I use are non-simultaneous, often with many years between the measurements in different

bands. Variations by factors of a few in each band are common over these time-scales in low-luminosity objects (see, e.g., M05, and references therein). This uncertainty should be kept in mind when comparing the non-simultaneous measurements of each individual object to the mean quasar SEDs.

The sample of LINERs discussed here has been selected to be unobscured, in the sense that a nuclear UV point source is detected, optical imaging, when available, has not show evidence for foreground dust extinction, and X-ray absorbing columns are $N_H \lesssim 10^{22} \text{ cm}^{-2}$. From Fig. 1, it is qualitatively evident that the SEDs of this sample are not dramatically different from those of quasars [the typical quasars used to produce the Elvis et al. (1994) templates have $\nu L_\nu(2500 \text{ Å}) \sim 10^{45} \text{ erg s}^{-1}$]. While the ratio of X-ray to UV luminosity is sometimes larger in the LINERs, the difference is by not by more than a factor of a few. Furthermore, there is no clear evidence for the absence of an optical-UV bump, only perhaps some signs that such a bump may be weaker, relative to X-rays, compared to quasars.

In the radio, Fig. 1 confirms previous assessments that, compared to quasars, most low-luminosity AGNs are radio loud, or even “super radio loud”. The radio loudness and UV-to-X ratio are examined more quantitatively below.

5.2 α_{ox}

Figure 2 permits a more quantitative look at the UV-to-X ratio by showing α_{ox} as a function of UV luminosity. For every object in the LINER sample, I plot the two α_{ox} values obtained by using either the high UV point or the UV lower limit, and connect them with a line. The true α_{ox} is therefore somewhere along these connecting lines, but possibly even below the point corresponding to the highest UV measurement, because UV measurements are so susceptible to extinction. We thus see that α_{ox} for most of the sample spans the range $-1.4 < \alpha_{ox} < -0.8$. [I note that the values of α_{ox} for the four objects in common to Ho (1999) and

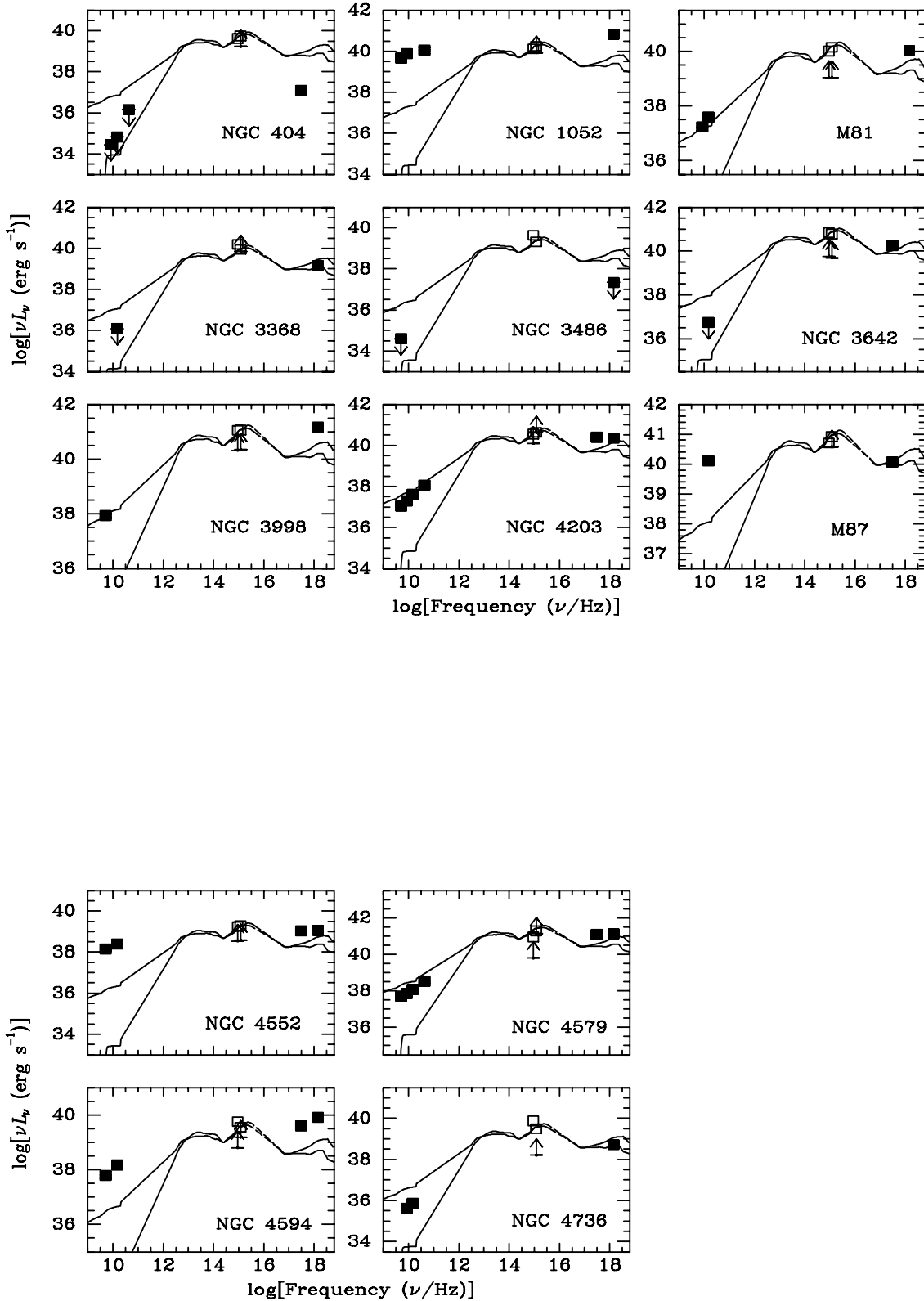


Figure 1. Radio through X-ray spectral energy distributions for the 13 LINERs, in $\log \nu L_\nu$ vs. $\log \nu$. Upper limits are 3σ . Lower limits in the UV are based on the variable, and hence nonstellar, flux. The solid curves show the mean SEDs of radio-loud and radio-quiet quasars from Elvis et al. (1994), normalized to pass through the high UV 2500 Å measurement of each LINER.

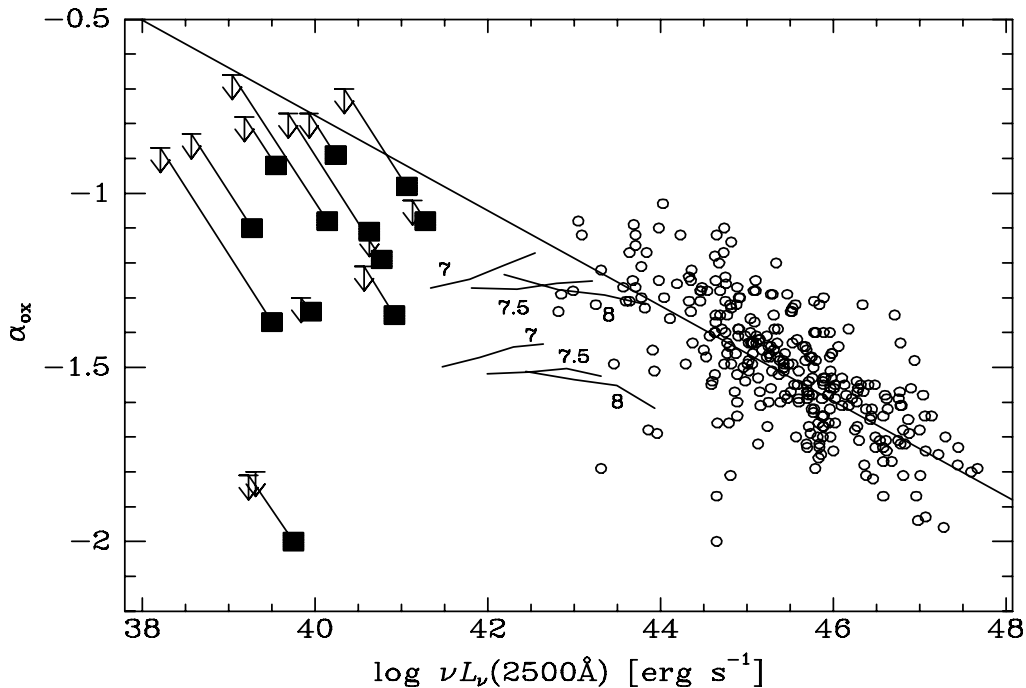


Figure 2. The UV-to-X-ray spectral index, α_{ox} , vs. 2500 Å luminosity, $\nu L_{\nu}(2500 \text{ \AA})$. For every LINER, the value obtained by using its high UV point is shown with a filled square, the value based on its UV lower limit is marked as an upper limit on α_{ox} , and the two are connected with a line. Small symbols reproduce the compilation by Steffen et al. (2006) of α_{ox} and 2500 Å luminosity for several samples of broad-lined AGNs. The best-fitting trend between these variables found by these authors for their sample is also shown (straight line). The α_{ox} values for most of the LINER sample span the range $-1.4 < \alpha_{\text{ox}} < -0.8$, largely overlapping with that of the Seyferts in the Steffen et al. sample. The short curves are from models by Merloni & Fabian (2002) of coronal outflow dominated thin accretion discs (see §6). Each curve is labelled by its black hole mass, $\log(M_{\text{BH}}/M_{\odot})$. The accretion rate along each curve decreases from $10^{-2} L_E$ on the right end to $10^{-3.5} L_E$ on the left. Models are shown for two values of the numerical factor K , which contains the unknown quantities in the model, and is related to the maximal fraction of power released in the corona. The top three curves are for $K = 0.95$ and the bottom three are for $K = 0.775$.

to this work (M81, M87, NGC 4579, NGC 4594) are similar. Thus, the X-ray fluxes used by Ho (1999), which were based on *Einstein*, *Rosat*, and *ASCA* measurements having lower angular resolutions, did not significantly overestimate the AGN flux, due to inclusion of diffuse X-ray emission or discrete circumnuclear sources.]

To place these results in the wider AGN context, I reproduce in Fig. 2 the compilation by Steffen et al. (2006) of α_{ox} and 2500 Å luminosity for several samples of broad-lined AGNs. Also plotted (straight line) is the best-fitting trend between these variables, as found by Steffen et al. (2006) for their sample. While the α_{ox} values for the LINERs are high compared to those of luminous quasars, as we saw quantitatively in Fig. 1 (most of the quasars in the Elvis et al. 1994 sample have $-1.5 < \alpha_{\text{ox}} < -1.2$), they are actually *in a similar range to those of Seyfert 1 galaxies*, having luminosities up to $\sim 10^{44} \text{ ergs s}^{-1}$. The α_{ox} 's of the LINERs are clearly below the extrapolation of the Steffen et al. relation to low luminosities. Indeed, based on their data alone, Steffen et al. already noted evidence (significant at the 2σ level) for a flattening of the relation toward low luminosities. Figure 2 shows that such a turnover is unavoidable. We thus see that unobscured low-luminosity AGNs, as far as their UV-to-X

luminosity ratios are concerned, are quite similar to AGNs that are 10^4 times more luminous in UV and X-rays.

Two galaxies, NGC 404 and NGC 3486, are very faint or undetected in X-rays, leading to outlying low values of α_{ox} . Interestingly, both galaxies have small expected BH masses, of $\lesssim 10^6 M_{\odot}$, an order of magnitude or more below those of the rest of the sample. A larger sample of galaxies is required to see if such a trend, of underluminous X-ray sources from small bulges, is real. One must keep in mind also the possibility that both of these objects are not true AGNs, and that the nuclear UV sources are, instead, compact star clusters. Maoz et al. (1998) indeed found that at least some of the UV light in NGC 404 is from massive stars. Although M05 found that the UV flux in NGC 404 differed significantly between their single epoch and previous HST observations, there is always some risk in such comparisons among measurements made with different instrumental setups. As noted above, NGC 3486 has not been seen to vary on either long or short time-scales, and so a nonstellar nature of its UV emission has not been demonstrated. (In fact, since it is also undetected in radio, its optical spectrum, showing a borderline LINER/Seyfert 2 nucleus, is the only indicator of a possible AGN.) Further data are thus needed in order to determine if such objects are powered by stars, or constitute another

AGN phase, characterized by very steep α_{ox} , and perhaps limited to galaxies with small BHs.

5.3 Radio Loudness

Figure 3 plots the radio-loudness parameter, R_{UV} , vs. UV luminosity for the LINER sample. As in Fig. 2, the two possible values, based on the two UV measurements, are shown for every galaxy, and are connected by lines. For comparison, I include in Fig. 3 data from the recent compilation by Sikora et al. (2007) for several AGN samples. I convert the luminosities and R parameters, which are given by Sikora et al. for the B -band (4400 Å), to 2500 Å, assuming an optical-UV power-law relation $f_{\nu} \propto \nu^{-0.5}$. The Sikora et al. (2007) points for the four LINERs in common with my sample (M81, NGC 3998, NGC 4203, NGC 4579) are not plotted. Figure 4 is the same as Figure 3, except that the two values of the UV luminosity for each object are normalized by the object’s Eddington luminosity. (Note that Sikora et al., in their fig. 4, plot R only versus the Eddington ratio, L/L_E , rather than L . However, as seen by comparing the Sikora et al. data in my Figs. 3 and 4, the plot is hardly changed when using either L or L/L_E , the result of the relatively small range in BH masses, compared to the large range in luminosities in their sample.)

Sikora et al. (2007) noted that, as pointed out by Ho (2002), radio loudness in inversely correlated with Eddington ratio. They showed, however, that the entire (possibly bimodal) distribution in R_{UV} , including both radio loud and radio quiet objects, shifts to higher R values when going from high to low luminosities. The radio-loud “branch” in the distribution consists exclusively of massive elliptical galaxies, with correspondingly large BHs, while the radio-quiet branch included both spirals and ellipticals. Related results have been shown by Xu et al. (1999), Laor (2001), Best et al. (2005), Wang, Wu, & Kong (2006), and Panessa et al. (2007).

The LINERs in the present sample conform with this picture. While their radio-to-UV luminosity ratios are often similar to those of radio-loud quasars, and sometimes even greater (as already seen qualitatively in Fig. 1), these AGNs fall on the same two branches on the diagram, with the majority actually being on the “radio-quiet” branch, with $\log R_{\text{uv}} \approx 2$. (I note that, in their compilation of radio fluxes, Sikora et al. 2007 included extended radio flux, while I have made a point of isolating, at the highest spatial resolution possible, just the unresolved nuclear flux. Inclusion of the extended flux in the LINER sample would likely move some of the points upwards in the diagram to some degree, but probably not by a large amount, since these are all core-dominated radio sources.) The four LINERs that are on the “radio-loud branch”, with $\log R_{\text{uv}} \approx 4$, (NGC 1052, M87, NGC 4552, and NGC 4594) indeed all have high BH masses, above $10^8 M_{\odot}$, and two of them have masses $> 10^9 M_{\odot}$. Equivalently, all the objects on the radio-loud branch have the lowest Eddington ratios, $\nu L_{\nu}(2500 \text{ Å})/L_E \lesssim 10^{-6}$.

Thus, in terms of their ratios of radio to UV luminosities, low-luminosity LINERs are, again, similar to AGNs of high luminosity, in that their radio loudness spans about 4 orders of magnitude, most of them are at the low- R end of the distribution, and the most radio-loud cases occur in massive early-type galaxies.

6 DISCUSSION AND CONCLUSIONS

The optical-to-UV emission in luminous AGNs is widely thought to come from the inner parts of a thermally radiating, geometrically thin, accretion disc. If so, this emission provides the most direct measure of the accretion rate on to the BH. Tracking this measure to lower and lower luminosities requires reliance on the UV, which is less susceptible than the optical emission to contamination by the old stellar population of galaxy bulges.

I have used new, high-angular-resolution data, particularly recent measurements and variability-based lower limits in the UV, to re-assess the SED of low-luminosity LINER nuclei. I have shown that, when focusing on unobscured objects, and when the faint nuclear emission is properly isolated from surrounding contamination, the SEDs of LINERs are similar to those of Seyfert-type AGNs 10^2 to 10^4 more luminous. This similarity is seen quantitatively in the parameters α_{ox} and R_{UV} . The lack of any conspicuous “phase transition” as a function of luminosity or accretion rate in the SEDs of LINERs, extends similar recent result by Panessa et al. (2007) for low-luminosity Seyferts.

It is tempting to speculate, therefore, that the same combination of physical components that gives rise to the SEDs of quasars is present at luminosities and accretion rates that are $\sim 10^{5-8}$ times smaller. In particular, if radiatively efficient accretion discs produce the UV emission in quasars, there is no compelling evidence that such discs disappear at low luminosities. Instead, the ratio of UV to X-ray emission is fairly insensitive to luminosity. It is only the ratio of luminosities between radio and other wavelengths that does increase dramatically as the luminosity decreases. However, it seems that the entire distribution of radio loudness shifts to higher values, with most objects remaining at the low side of the R distribution. The decrease in the accretion rate on to a supermassive BH (as traced by the UV luminosity) could thus be manifest as a hand-in-hand decrease in the UV and X-ray luminosities, but with a much smaller decrease in radio luminosity. The sources of the UV radiation (presumably a thin accretion disc) and of the X-rays apparently persist, but are simply scaled down, with a minor increase in the prominence of the X-ray emission.

Interestingly, analogous results have been found recently for stellar-mass Galactic BHs. Miller et al. (2006a,b) have analysed data for three BHs (including a re-analysis of *ASCA* data for Cygnus X-1 in its low state) accreting at $\sim 10^{-2}$ to $\sim 10^{-3}$ of the Eddington rate. In each case, the soft X-ray spectra require the presence of a thermally radiating thin accretion disc, down to the innermost marginally stable circular orbit. There is no obvious reason why such “mass-starved” structures could not exist at even-lower accretion rates. RIAFs were devised in order to explain the low luminosities that are observed from dormant galactic nuclei, despite the significant rates of mass infall expected on to the BHs. Instead, the evidence for the persistence of thin, radiatively efficient, but mass-flow-starved, discs suggests that some mechanism prevents gas from reaching the inner parts of the accretion flow in the first place. The radio loudness at low luminosities points to a solution in which gas joins a jet or outflow long before reaching the innermost orbits. High-resolution radio images of M87 indeed reveal a

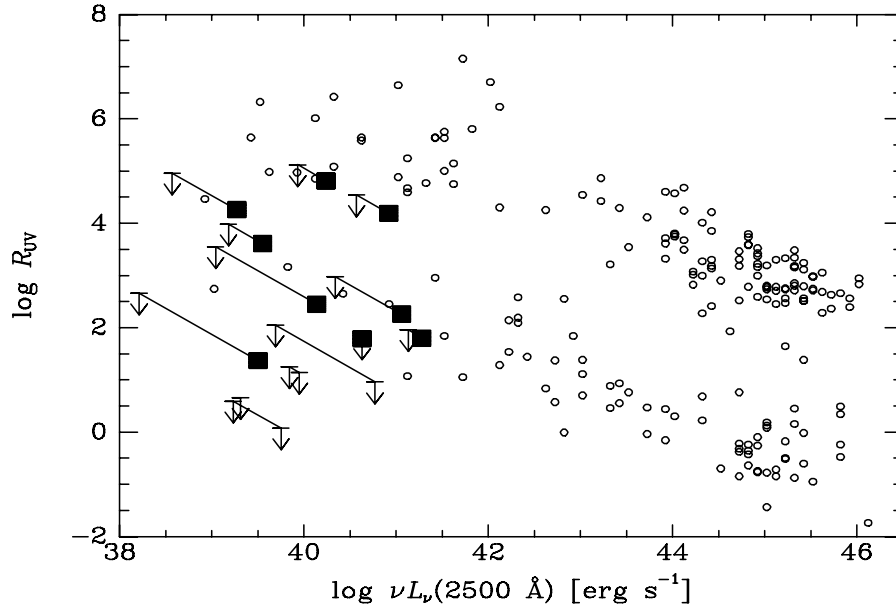


Figure 3. The radio-to-UV (5 GHz to 2500 Å) radio loudness parameter R_{UV} , plotted vs. 2500 Å luminosity, $\nu L_\nu(2500 \text{ \AA})$. As in Fig 2, R_{UV} using each LINER’s high UV point is shown with a filled square, R_{UV} based on the UV lower limit is marked as an upper limit, and the two are connected with a line. Double connected upper limits are based on the two UV measurements for objects that are undetected in radio. The single upper limit is NGC 3486, which is undetected in radio, and has no variability-based UV lower limit. Small symbols reproduce the compilation by Sikora et al. (2007) of R and L_B for several samples of AGNs, after converting their values from 4400 Å to 2500 Å. While all low-luminosity AGNs are, on average, radio-louder by a factor ~ 100 than high-luminosity quasars, most of the LINERs are actually on the “radio-quiet” branch of the distribution at low luminosities.

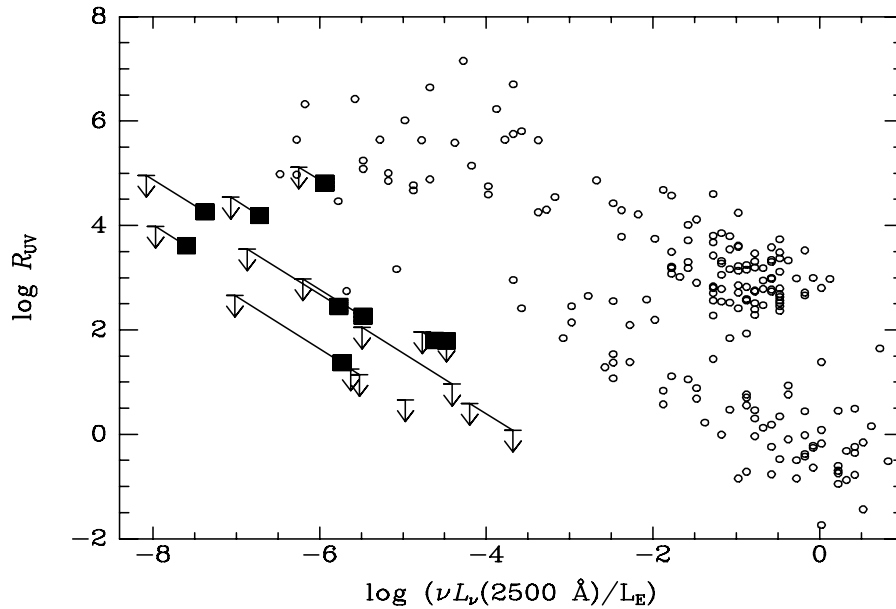


Figure 4. Same as Fig. 3, but normalizing the UV luminosity of each object by its Eddington luminosity, L_E .

very wide base for the jet, of order $100R_S$ or more (Junor et al. 1999; Ly et al. 2007), suggestive of this picture.

From a theoretical perspective, a recent model that may produce the essential features required by these data is the coronal outflow dominated accretion disc by Merloni & Fabian (2002). In this model, the magnetic stresses inside a geometrically thin, optically thick, disc generate an unbound magnetic corona. The corona comptonizes the thermal emission from the disc, producing the X-ray emission, and serves as a base for launching a vertical outflow or jet. At progressively lower accretion rates on to the BH, the ratio of the thermal to comptonized X-ray emission decreases, and the fraction of the gravitational potential energy channelled into kinetic energy of the outflow increases. Figure 2 shows, alongside the data, some of these models (kindly provided by A. Merloni) in the $\alpha_{\text{ox}} - \nu L\nu(2500 \text{ \AA})$ plane. Each curve in the plot is labelled by its BH mass, $\log(M_{\text{BH}}/M_{\odot})$. The accretion rate along each curve decreases from right to left, producing a bolometric luminosity of $10^{-2}L_E$ on the right, and going to $10^{-3.5}L_E$ on the left. Models are shown for two values of the numerical factor K , which contains the unknown quantities in the model – the viscosity, and the efficiency of buoyant transport of magnetic structure in the vertical direction inside the disc. K is thus related to the maximal fraction of power released in the corona. The top three curves are for $K = 0.95$ and the bottom three are for $K = 0.775$. Merloni & Fabian (2002) note that, at accretion rates below those corresponding to $L = 10^{-3.5}L_E$, the spectral shape remains unchanged, and the total luminosity simply goes down. From Fig. 2, it appears that large values of K (corresponding to high viscosity and high vertical speed) can lead to α_{ox} values comparable to those observed for the LINERs in the present sample. Furthermore, as the accretion rate decreases, the outflow becomes energetically more dominant. The radiation from this outflow/jet could then lead to the observed increase in R_{UV} at low luminosities.

Like many previous accretion models, the Merloni & Fabian (2002) model begins with a dynamical scenario, makes some assumptions, and includes free parameters that can be adjusted to achieve agreement with observations. An alternative approach has been taken recently by Loeb & Waxman (2007), who analyse the millimetre-band emission from Sag A*. Using measurements of size vs. wavelength of Sag A*, they conclude that, irrespective of the dynamics, geometry, and physical details of the gas flow, a net inflow toward the BH is likely only in the inner tens of Schwarzschild radii, whereas a net outflow is suggested at larger radii. Sag A* has an even lower Eddington ratio than the LINERs considered in this work, and it is of course unknown what its optical spectrum would be (LINER or otherwise), were we to view it from outside the obscuring disc of the Galaxy. None the less, the same theme recurs in the Loeb & Waxman (2007) analysis – a low net accretion rate on to the BH, with most of the accreting mass at large radii ending up in an outflow. This picture is in contrast to that invoked in many RIAF models, where the accretion energy of the mass inflow is advected into the BH.

To summarize, I have compiled recent radio, UV, and X-ray data for a sample of 13 unobscured low-luminosity LINER AGNs. I have shown that their interband luminosity ratios are not dramatically different from those of higher

luminosity AGNs. Specifically, in terms of their UV/X ratios, there is only a slightly enhanced prominence of the X-ray emission compared to Seyferts and quasars. There is thus no obvious indication for the disappearance of the big blue bump at low luminosities, suggesting the persistence of thin accretion discs in the low-accretion-rate regime. In terms of radio/UV luminosity ratios, the LINERs span a range of 4 orders of magnitude, with most of them residing at the lower end of the distribution, with $\log R_{\text{UV}} \lesssim 2$. In this sense, these low-luminosity AGNs again are part of a continuous sequence with higher luminosity objects. Since at least some, if not all, of the radio emission in AGNs is known to come from jets, this suggests a picture in which, at decreasing accretion rates, a progressively larger fraction of the inflowing mass is channelled into an outflow, and a smaller fraction into the persistent thin accretion disk. Analogous results have been obtained recently for some Galactic stellar-mass BHs.

While I have made an effort to compile the best available data, the measurements analyzed here are still crude. In particular, the fact that the measurements in different bands are often separated by years, coupled with the large fluctuations in flux that are common in low-luminosity AGNs, means that individual luminosity ratios could be off by an order of magnitude. Future improvements could be achieved by means of contemporaneous X-ray and UV data, which could possibly be obtained using the multi-band capabilities on *Newton-XMM* or *SWIFT* (for sources with an X-ray flux $\gtrsim 10^{-13} \text{ erg cm}^{-2} \text{ s}^{-1}$), and could be complemented by simultaneous ground-based radio data. Repeated observations of individual objects over few-year time-scales could reveal changes in SED as a function of changing luminosity. Such monitoring would also reduce the uncertainty regarding the non-stellar contribution to the UV, another major source of error in the present work. Detection of nuclear variability also in the optical (with HST) and in the IR (with *Spitzer*) would permit measuring reliably the AGN component in those bands as well, significantly sharpening our view of the SED. Finally, much larger samples of unobscured low-luminosity AGNs, analyzed in similar ways, could clarify the picture considerably. A larger, UV-selected, sample of such objects could be assembled by means of UV imaging (e.g., with *GALEX* or with HST) and subsequent optical spectroscopic classification to identify the LINERs. UV imaging need not necessarily be from space – the UV nuclei of the current sample are prominent in the F330W band, so such objects could potentially be identified by ground-based observations near the atmospheric UV cutoff. Alternatively, one could begin with the large, optically selected, SDSS LINER sample of Kewley et al. (2006), and follow it up with sensitive multiwavelength observations.

ACKNOWLEDGMENTS

I thank Ari Laor and Brent Groves for very useful suggestions and discussions. Andrea Merloni is thanked for making his models available in digital form. This research has made use of the NASA/IPAC Extragalactic Database (NED) which is operated by the JPL, Caltech, under contract with NASA.

REFERENCES

Anderson, J. M., Ulvestad, J. S., & Ho, L. C. 2004, *ApJ*, 603, 42

Barth, A. J. & Shields, J. C. 2000, *PASP*, 112, 753

Barth, A. J., Reichert, G. A., Filippenko, A. V., Ho, L. C., Shields, J. C., Mushotzky, R. F., and Puchnarewicz, E. M. 1996, *AJ*, 112, 1829

Barth, A. J., Reichert, G. A., Ho, L. C., Shields, J. C., Filippenko, A. V., & Puchnarewicz, E. M. 1997, *AJ*, 114, 2313

Barth, A. J., Ho, L. C., Filippenko, A. V., & Sargent, W. L. W. 1998 *ApJ*, 496, 133

Best, P. N., Kauffmann, G., Heckman, T. M., & Ivezić, Ž. 2005, *MNRAS*, 362, 9

Bietenholz, M. F., Bartel, N., & Rupen, M. P. 2000, *ApJ*, 532, 895

Biretta, J. A., Stern, C. P., & Harris, D. E. 1991, *AJ*, 101, 1632

Bower, G. A., Wilson, A. S., Heckman, T. M., Magorrian, J., Gebhardt, K., Richstone, D. O., Peterson, B. M., & Green, R. F. 2000, *BAAS*, 32, 1566

Cappellari, M. et al. 1999, *ApJ*, 519, 117

Cappi, M., et al. 2006, *A&A*, 446, 459

Chiaberge, M., Capetti, A., & Macchetto, F. D. 2005, *ApJ*, 625, 716

Chiaberge, M., Gilli, R., Macchetto, F. D., & Sparks, W. B. 2006, *ApJ*, 651, 728

Cardelli, J. A., Clayton, G. C., & Mathis, J. S. 1989, *ApJ*, 345, 245

de Francesco, G., Capetti, A., & Marconi, A. 2006, *A&A*, 460, 439

Devereux, N., Ford, H., & Jacoby, G. 1997, *ApJ*, 481, L71

Devereux, N., Ford, H., Tsvetanov, Z., & Jacoby, G. 2003, *AJ*, 125, 1226

Di Matteo, T., Johnstone, R. M., Allen, S. W., & Fabian, A. C. 2001, *ApJ*, 550, L19

Di Matteo, T., Allen, S. W., Fabian, A. C., Wilson, A. S., & Young, A. J. 2003, *ApJ*, 582, 133

Done, C., & Gierliński, M. 2005, *Ap&SS*, 300, 167

Dunn, R. J. H., & Fabian, A. C. 2006, *MNRAS*, 373, 959

Elvis, M., et al. 1994, *ApJS*, 95, 1

Eracleous, M., Shields, J. C., Chartas, G., & Moran, E. C. 2002, *ApJ*, 565, 108

Fabbiano, G., Fassnacht, C., & Trinchieri, G. 1994, *ApJ*, 434, 67

Falcke, H. & Biermann, P. L. 1999, *A&A*, 342, 49

Falcke, H., Nagar, N.M., Wilson, A.S., & Ulvestad, J.S. 2000, *ApJ*, 542, 197

Falcke, H., Körding, E., & Markoff, S. 2004, *A&A*, 414, 895

Filho, M. E., Barthel, P. D., & Ho, L. C. 2002, *A&A*, 385, 425

Flohic, H. M. L. G., Eracleous, M., Chartas, G., Shields, J. C., & Moran, E. C. 2006, *ApJ*, 647, 140

Gabel, J. R., Bruhweiler, F. C., Crenshaw, D. M., Kraemer, S. B., & Miskey, C. L. 2000, *ApJ*, 532, 883

Graham, D. A., Weiler, K. W., & Wielebinski, R. 1981, *A&A*, 97, 388

Guainazzi, M., Oosterbroek, T., Antonelli, L. A., & Matt, G. 2000, *A&A*, 364, L80

Häring, N., & Rix, H.-W. 2004, *ApJ*, 604, L89

Heckman, T. M. 1980, *A&A*, 87, 152

Heinz, S., Merloni, A., & Schwab, J., 2007, *ApJL*, in press, astro-ph/0702211

Ho, L. C. 1999, *ApJ*, 516, 672

Ho, L. C. 2002, *ApJ*, 564, 120

Ho, L. C. & Ulvestad, J. S. 2001, *ApJS*, 133, 77

Ho, L. C., Filippenko, A. V., & Sargent, W. L. W. 1996, *ApJ*, 462, 183

Ho, L. C., Filippenko, A. V., & Sargent, W. L. W. 1997, *ApJS*, 112, 315

Ho, L. C., et al. 2001, *ApJ*, 549, L51

Hummel, E., van der Hulst, J. M., & Dickey, J. M. 1984, *A&A*, 134, 207

Junor, W., Biretta, J. A., & Livio, M. 1999, *Nature*, 401, 891

Kadler, M., Kerp, J., Ros, E., Falcke, H., Pogge, R. W., & Zensus, J. A. 2004, *A&A*, 420, 467

Kaspi, S., Smith, P. S., Netzer, H., Maoz, D., Jannuzi, B. T., & Giveon, U. 2000, *ApJ*, 533, 631

Kauffmann, G., et al. 2003, *MNRAS*, 346, 1055

Kellermann, K. I., et al. 2004, *ApJ*, 609, 539

Kewley, L. J., Groves, B., Kauffmann, G., & Heckman, T. 2006, *MNRAS*, 372, 961

Kishimoto, M., Antonucci, R., & Blaes, O. 2005, *MNRAS*, 364, 640

Kollmeier, J. A., et al. 2006, *ApJ*, 648, 128

Komossa, S., Böhringer, H., & Huchra, J. P. 1999, *A&A*, 349, 88

Koratkar, A., Deustua, S. E., Heckman, T., Filippenko, A. V., Ho, L. C., & Rao, M. 1995, *ApJ*, 440, 132

Körding, E., Colbert, E., & Falcke, H. 2005, *A&A*, 436, 427

Körding, E., Falcke, H., & Corbel, S. 2006, *A&A*, 456, 439

Kormendy, J., et al. 1996, *ApJ*, 473, L91

Laor, A. 2001, *ApJ*, 553, 677

Loeb, A., & Waxman, E. 2007, astro-ph/0702043

Ly, C., Walker, R. C., & Junor, W. 2007, *ApJ*, in press, astro-ph/0701511

Macchetto, F., Marconi, A., Axon, D. J., Capetti, A., Sparks, W., & Crane, P. 1997, *ApJ*, 489, 579

Machacek, M., Nulsen, P. E. J., Jones, C., & Forman, W. R. 2006, *ApJ*, 648, 947

Malkan, M. A. 1983, *ApJ*, 268, 582

Maoz, D., Filippenko, A. V., Ho, L. C., Rix, H.-W., Bahcall, J. N., Schneider, D. P., and Macchetto, F. D. 1995, *ApJ*, 440, 91

Maoz, D., Filippenko, A.V., Ho, L.C., Macchetto, F.D., Rix, H.-W., & Schneider, D.P. 1996, *ApJS*, 107, 215

Maoz, D., Koratkar, A. P., Shields, J. C., Ho, L. C., Filippenko, A. V., & Sternberg, A. 1998, *AJ*, 116, 55

Maoz, D., Nagar, N. M., Falcke, H., & Wilson, A. S. 2005, *ApJ*, 625, 699 (M05)

Marconi, A., Risaliti, G., Gilli, R., Hunt, L. K., Maiolino, R., & Salvati, M. 2004, *MNRAS*, 351, 169

Merloni, A., & Fabian, A. C. 2002, *MNRAS*, 332, 165

Miller, J. M., Homan, J., & Miniutti, G. 2006, *ApJ*, 652, L113

Miller, J. M., Homan, J., Steeghs, D., Rupen, M., Hunstead, R. W., Wijnands, R., Charles, P. A., & Fabian, A. C. 2006, *ApJ*, 653, 525

Nandra, K., O'Neill, P. M., George, I. M., Reeves, J. N., & Turner, T. J. 2006, *Astronomische Nachrichten*, 327, 1039

Nagar, N.M., Falcke, H., Wilson, A.S., & Ho, L.C. 2000, *ApJ*, 542, 186

- Nagar, N. M., Wilson, A. S., & Falcke, H. 2001, *ApJ*, 559, L87
- Nagar, N.M., Wilson, A.S., Falcke, H., & Ulvestad, J.S. 2002, *A&A*, 392, 53
- Nagar, N. M., Falcke, H., & Wilson, A. S. 2005, *A&A*, 435, 521
- Netzer, H., & Trakhtenbrot, B. 2007, *ApJ*, 654, 754
- Nicholson, K. L., Reichert, G. A., Mason, K. O., Puchanewicz, E. M., Ho, L. C., Shields, J. C., & Filippenko, A. V. 1998, *MNRAS*, 300, 893
- Nusser, A., Silk, J., & Babul, A. 2006, *MNRAS*, 373, 739
- Panessa, F., Bassani, L., Cappi, M., Dadina, M., Barcons, X., Carrera, F. J., Ho, L. C., & Iwasawa, K. 2006, *A&A*, 455, 173
- Panessa, F., Barcons, X., Bassani, L., Cappi, M., Carrera, F. J., Ho, L. C., & Pellegrini, S. 2007, *A&A*, in press, astro-ph/0701546
- Pellegrini, S., Venturi, T., Comastri, A., Fabbiano, G., Fiore, F., Vignali, C., Morganti, R., & Trinchieri, G. 2003a, *ApJ*, 585, 677
- Pellegrini, S., Baldi, A., Fabbiano, G., & Kim, D.-W. 2003b, *ApJ*, 597, 175
- Perlman, E. S., Harris, D. E., Biretta, J. A., Sparks, W. B., & Macchetto, F. D. 2003, *ApJ*, 599, L65
- Pietsch, W., & Read, A. M. 2002, *A&A*, 384, 793
- Pogge, R.W., Maoz, D., Ho, L.C., & Eracleous, M. 2000, *ApJ*, 532, 323
- Ptak, A., Terashima, Y., Ho, L. C., & Quataert, E. 2004, *ApJ*, 606, 173
- Quataert, E., di Matteo, T., Narayan, R., & Ho, L. C. 1999, *ApJ*, 525, L89
- Roberts, T. P. & Warwick, R. S. 2000, *MNRAS*, 315, 98
- Sarzi, M., et al. 2002, *ApJ*, 567, 237
- Satyapal, S., Sambruna, R. M., & Dudik, R. P. 2004, *A&A*, 414, 825
- Schlegel, D. J., Finkbeiner, D. P., & Davis, M. 1998, *ApJ*, 500, 525
- Shakura, N. I. & Sunyaev, R. A. 1973, *A&A*, 24, 337
- Shang, Z., et al. 2005, *ApJ*, 619, 41
- Shankar, F., Salucci, P., Granato, G. L., De Zotti, G., & Danese, L. 2004, *MNRAS*, 354, 1020
- Shields, G. A. 1978, *Nature*, 272, 706
- Silk, J. 2005, *MNRAS*, 364, 1337
- Sikora, M., Stawarz, L., & Lasota, J. -P. 2007, *ApJ*, in press, astro-ph/0604095
- Soltan, A. 1982, *MNRAS*, 200, 115
- Soria, R., Fabbiano, G., Graham, A. W., Baldi, A., Elvis, M., Jerjen, H., Pellegrini, S., & Siemiginowska, A. 2006a, *ApJ*, 640, 126
- Soria, R., Graham, A. W., Fabbiano, G., Baldi, A., Elvis, M., Jerjen, H., Pellegrini, S., & Siemiginowska, A. 2006b, *ApJ*, 640, 143
- Springel, V., Di Matteo, T., & Hernquist, L. 2005, *ApJ*, 620, L79
- Steffen, A. T., Strateva, I., Brandt, W. N., Alexander, D. M., Koekemoer, A. M., Lehmer, B. D., Schneider, D. P., & Vignali, C. 2006, *AJ*, 131, 2826
- Sturm, E., et al. 2006, *ApJ*, 653, L13
- Terashima, Y., Ho, L. C., & Ptak, A. F. 2000, *ApJ*, 539, 161
- Terashima, Y. & Wilson, A. S. 2003, *ApJ*, 583, 145
- Terashima, Y., Iyomoto, N., Ho, L. C., & Ptak, A. F. 2002, *ApJS*, 139, 1
- Tremaine, S., et al. 2002, *ApJ*, 574, 740
- Volonteri, M., Salvaterra, R., & Haardt, F. 2006, *MNRAS*, 373, 121
- Wang, R., Wu, X.-B., & Kong, M.-Z. 2006, *ApJ*, 645, 890
- Wilson, A. S., & Yang, Y. 2002, *ApJ*, 568, 133
- Xu, C., Livio, M., & Baum, S. 1999, *AJ*, 118, 1169
- Yuan, F. 2007, in "The Central Engine of Active Galactic Nuclei", eds. L. C. Ho and J.-M. Wang (San Francisco: ASP), astro-ph/0701638
- Yuan, F., Markoff, S., Falcke, H., & Biermann, P. L. 2002, *A&A*, 391, 139